Int. J. Electrochem. Sci., 13 **(2018)** 10427 – 10439, doi: 10.20964/2018.11.46

International Journal of
ELECTROCHEMICAL
SCIENCE
www.electrochemsci.org

A First Principle Study of Electronic Structure and Site Occupancy of Cation doped $LiFePO_4$ Cathode Material

Hong Liang Zhang[1], *Yang Gong*[1], *Shuai Yang*[2], *Jie Li*[1,*], *Ke Du*[1], *JiaQi Li*[1]

[1] School of Metallurgy and Environment, Central South University, Changsha 410083, PR China
[2]College of Mechanical and Electrical Engineering, Yangtze Normal University, Chongqing 408100, P R China
[*]E-mail: 163512087@csu.edu.cn

Received: 18 June 2018 / *Accepted:* 30 August 2018 / *Published:* 1 October 2018

Cation doping could be adopted as an effective method to optimize the electrochemical performance of Li-ion battery cathode materials. However, there is still major controversy regarding the site occupation behavior in the lattice following cation doping. To determine the preferred dopant sites in $LiFePO_4$ and the general relation with ionic charge and/or size, density functional theory (DFT) was adopted to calculate the models of a range of dopants with charges varying from +1 to +6 doped at the Fe site or Li site of $LiFePO_4$. As a result, it was found that cations preferentially occupy the Fe sites in a thermodynamically spontaneous process due to the stronger covalent interaction between dopants and adjacent O atoms; ionic charge is the dominant factor affecting the doping site occupation behavior, and ionic size is secondary. In addition, the doping of Fe sites preferentially favors the doping of high-valence ions, while the Li sites are more susceptible to low-valent ion dopants. From an energy standpoint, cation doping is more favorable with non-transition metal ions than with transition metal ions in both Fe and Li sites. The calculation results are consistent with the related experimental results.

Keywords: Cathode material; Site occupation behavior; Cation doping; Density Functional Theory;

1. INTRODUCTION

Portable electronic devices, electric vehicles, hybrid electric vehicles, and distributed energy storage systems place high energy density demands on rechargeable batteries, thus motivating theoretical and experimental research on lithium-ion batteries [1-4]. Since first reported by Goodenough [5] as a cathode material, $LiFePO_4$ has attracted extensive research interest due to its safety, high specific discharge capacity, environmental friendliness and low cost. However, one of the key drawbacks with using $LiFePO_4$ is its low intrinsic electronic (ion) conductivity, which makes the electron (ion)

migration in the cathode material during charge-discharge an electrochemically controlled process. Therefore, different methods have been employed to overcome this problem, including carbon coating [6-9], metal phosphide coating [10] and cation doping [11]. It should be pointed out that the carbon coating will reduce the tap density of the material, thereby reducing the volume energy density of the battery, while the metal phosphide coating will increase the resistance of the material in the process of lithium intercalation/deintercalation. Furthermore, carbon or phosphide coating can only impact the surface of the particles and cannot improve the intrinsic electron (ion) conductivity of the material.

To optimize the intrinsic conductivity of materials, considerable effort has been invested in doping ions into lattices. In particular, Chiang and his colleagues [11] first reported their results on doping polyvalent ions (Mg^{2+}, Al^{3+}, Ti^{4+}, Zr^{4+}, Nb^{5+}) and claimed that the electrical conductivity of bulk $LiFePO_4$ increased by 8 orders of magnitude, which is comparable to $LiCoO_2$ or $LiMn_2O_4$. Based on this initial exploration, experiments in which $LiFePO_4$ was doped with different ions were carried out. Potential dopants include divalent (Mg [12-14], Zn [15]), trivalent (Cr [16], Al [17]), tetravalent (Ti [18-20], Zr [21], Sn [22]), pentavalent (V [23, 24], Nb [25, 26]), and hexavalent ions (Mo [27]).

However, there is still some controversy regarding whether supervalent ions can be doped into the $LiFePO_4$ lattice and occupy preferred dopant sites (Fe site or Li site). In particular, Islam M S [28] conducted a relatively comprehensive theoretical study using atomistic simulations in the early stage and claimed that only divalent ions (e.g., Mn, Co, Ni) can be incorporated into the $LiFePO_4$ lattice with low energy favorable at the Fe site, while aliovalent doping of $LiFePO_4$ was unachievable. The results are in accordance with some previous experimental phenomena; however, in subsequent experimental [21,29] and theoretical studies [30], it was found that low levels of isovalent ions do indeed diffuse into the LiFePO4 lattice and can improve its electrochemical properties. Wagemaker M et al [29] studied the doping position of ultravalent ions (Zr, Nb, Cr) through neutron and X-ray diffraction experiments and found that low concentrations of dopants are indeed soluble in the olivine lattice up to the extent of 3%. Hoang K et al [30] investigated the lattice site preference of different dopant ions and its influence on the electronic and ionic conductivity of the host material, and the results showed that Na is energetically more favorable at the Li site, whereas Mg, Al, Zr, and Nb are more favorable at the Fe site. The inconsistency between Islam's simulation results [28] and subsequent experiments and/or calculations may be because charge compensation processes were not properly considered, thus leading to the conclusion that aliovalent dopants are insoluble. Therefore, in the calculation model constructed in this work, we mainly adopt two commonly accepted charge compensation mechanisms, that is, doping on the Li site is responsible for compensating for defects in the Li site [11,31], and doping on the Fe site causes Fe defects [32].

In this paper, first-principles calculations based on DFT were employed to systematically and extensively investigate whether a range of cations with charges varying from +1 to +6 can be incorporated into the $LiFePO_4$ lattice and what factors influence the preferred dopant sites and favorable occupancy. Then, from a ground state energy point of view, the ion occupancy situation was analyzed to rule out the possibility of obtaining inconsistent results due to different experimental synthesis conditions.

2. COMPUTATIONAL METHOD AND MODELS

In this work, first-principles calculations based on DFT were performed, as implemented in the CASTEP package [33]. The exchange–correlation (X–C) energy was treated within the generalized gradient approximation (GGA) of Perdew–Burke–Ernzerhof (PBE) [34]. Ultrasoft pseudo-potentials (USPP) introduced by Vanderbilt [35] were employed for all ion-electron interactions. The plane-wave cutoff energy was set at 520 eV. The gamma centered Monkhorst-Pack scheme of k-point generation was applied to grids of 2×3×2 for structural optimization and the final energy calculation. The structural optimization was performed with both lattices and internal coordinates fully relaxed. The total energy was converged to within 1×10^{-6} eV/atom.

For all models, to improve computational efficiency, a 1×1×2 supercell box was created. The CASTEP model is only suitable for system of tens of atoms, so the doping content was fixed as M:Fe=1:7 in this study. Although such a high doping concentration (12.5%) was not possible experimentally for some elements, it can surely provide a rough comprehension of the doping effects. It is interesting to note that for the doping of odd-number valence state ions (such as M^{3+} or M^{5+}) at the Fe site, 1×2×2 supercells were established in order to control the same doping concentration (12.5%) of all elements. Therefore, the volume of the doping system for +3 and +5 ions is about twice as large as that of the others, as shown in Table 1.

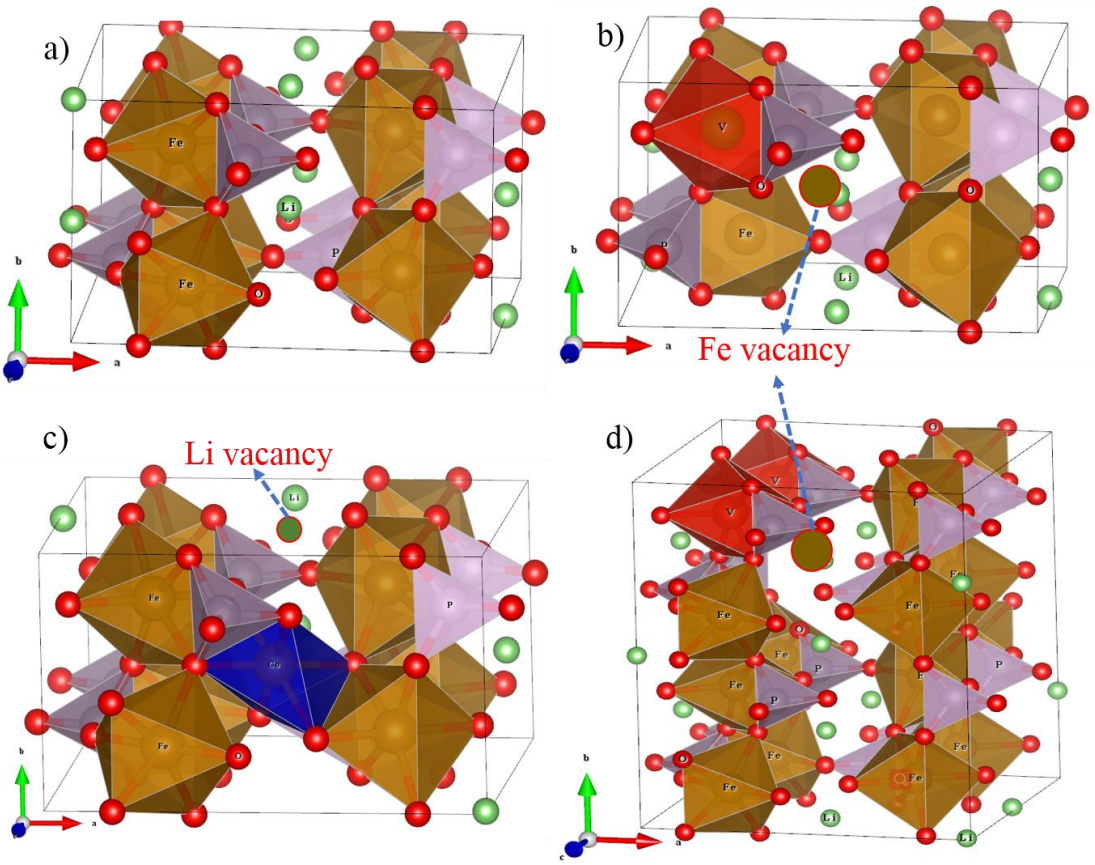

Figure 1. 1×1×2 supercell crystal structure of a) pristine $LiFePO_4$, b) V^{4+} doped at Fe sites creates a Fe vacancy, c) Co^{2+} doped at Li sites creates a Li vacancy, and d) 1×2×2 supercell crystal structure of V^{3+} at Fe sites creates a Fe vacancy.

Because impurities exist in the doped crystal pattern, one atom (Fe or Li atom) was replaced with another dopant atom M (M=Na^{+}, Mg^{2+}, Cu^{2+}, Ni^{2+}, Co^{2+}, Mn^{2+}, V^{2+}, Al^{3+}, V^{3+}, Co^{3+}, Ni^{3+}, Mn^{3+}, Zr^{4+}, V^{4+}, Nb^{5+}, V^{5+}, Mo^{6+}). Two commonly accepted charge compensation mechanisms were adopted to compensate for charge balance: doping at the Li (M1) site is responsible for compensating for defects in the Li (M1) site [11,29], and doping at the Fe (M2) site causes charge compensation defects to occur in the Fe (M2) site [32] at the nearest-neighbor dopant site [31], as shown in Fig. 1.

3. RESULTS AND DISCUSSION

3.1. Structural Analysis

$LiFePO_4$, with an olivine structure, belongs to the orthorhombic system and its space group is Pnma. O atoms form a slightly distorted hexagonal close packed structure, in which the P atoms and the surrounding O atoms form a PO_4 tetrahedron and occupy the 4c position of the tetrahedron. Li and Fe form LiO_6 and FeO_6 octahedra with the surrounding O atoms, respectively. In the b-axis direction, LiO_6 octahedra are connected side by side to form a chain, while the FeO_6 octahedra are connected at a common corner. In addition, one PO_4 tetrahedron is colocated with two LiO_6 octahedrons, two Fe atoms and one P atom in the $LiFePO_4$ structure sharing one O atom, as shown in Fig. 1(a).

Table 1 shows the lattice parameters and the volume of the crystal calculated by DFT. From Table 1, we can see that as the radius of the dopant ion increases, the volume of the crystals gradually increases, indicating that the dopant ions incorporate into the lattice and form a solid solution. In addition, ions with a similar radius (such as Nb^{5+}/V^{3+}, V^{5+}/Co^{3+}, Zr^{4+}/Mg^{2+}) are incorporated at the Fe site. Moreover, the greater the charges of the ions are, the larger the cell volume, which may be because with a greater charge, the system needs to make the unit cell expand so that the internal repulsion interactions between ions is minimal. In addition, this indicates that supervalent ionic doping at the Fe site can broaden the diffusion channel of lithium ions where, the opposite is true for Li site doping.

Table 1. The lattice parameter a, b, c and the volume (V) of M^{n+} (n=1~6) doped at the Fe site and Li site of $LiFePO_4$

Elements	charges	Ionic Radius (pm)	M^{n+} doped on Fe sites				M^{n+} doped on Li sites			
			a (Å)	b (Å)	c (Å)	V ($Å^3$)	a (Å)	b (Å)	c (Å)	V ($Å^3$)
Na	1	102			/		9.861	5.807	9.382	537.186
Co	2	65	9.864	5.793	9.320	532.579	9.862	5.749	9.305	527.594
Mn		67	9.864	5.793	9.320	532.589	9.852	5.754	9.310	527.773
Ni		69	9.866	5.805	9.330	534.329	9.863	5.744	9.335	528.878
Mg		72	9.891	5.814	9.328	536.501	9.857	5.766	9.338	530.752

Cu		73	9.887	5.819	9.335	537.041	9.874	5.757	9.344	531.186
V		79	9.874	5.832	9.334	537.490	9.864	5.772	9.342	531.931
Al		53.5	9.835	11.570	9.333	1061.963	9.845	5.737	9.251	522.481
Co		54.5	9.841	11.574	9.322	1061.814	9.855	5.719	9.281	523.100
Ni	3	56	9.844	11.631	9.337	1068.909	9.874	5.718	9.308	525.492
Mn		58	9.868	11.572	9.337	1066.173	9.836	5.729	9.299	523.985
Cr		61.5	9.868	11.574	9.324	1064.958	9.837	5.724	9.308	524.126
V		64	9.887	11.605	9.332	1070.758	9.784	5.736	9.355	525.058
V	4	58	9.886	5.801	9.348	536.084	9.751	5.702	9.334	518.961
Zr		72	9.970	5.884	9.401	551.549	9.789	5.751	9.413	529.891
V	5	54	9.896	11.616	9.361	1075.984	9.742	5.658	9.411	518.757
Nb		64	9.990	11.682	9.374	1093.968	9.725	5.672	9.460	521.815
Mo	6	59	9.978	5.839	9.380	546.418	9.717	5.627	9.406	514.306

3.2. Electronic Structure Analysis

To evaluate the effect of doping on the electronic structure and verify the reliability of the calculation results by comparison with current existing calculations and experimental results, common ions such as Mg^{2+}, Mn^{2+}, Al^{3+}, Cr^{3+}, V^{3+}, Zr^{4+}, Nb^{5+} and Mo^{6+} were doped at the Fe and Li sites. Their electronic structures were calculated, and the partial density of states (PDOS) are plotted in Fig. 2 and Fig. 3. From Fig. 2(a), it can be seen that for the pure $LiFePO_4$, the calculated bandgap is 0.74 eV, which is close to 0.62 eV reported previously using a similar method [32] and is slightly larger than the 0.53 eV value calculated by SQ Shi [31] and the 0.3 eV value calculated by Chung [11]; however, it is much smaller than the experimental value (3.75 eV) [36] due to the inaccurate handling of the GGA method for the interaction of the transition metal d orbital electrons. Although the calculated bandgap values for the GGA method are below the experimental values in most cases, good predictions can be made for orbital occupancy.

In the case of cation-doped $LiFePO_4$, the presence of impurities has a significant impact on the distributions of electron quantum states (as shown in Fig. 2 and Fig. 3). These extra electrons give rise to a larger DOS near the Fermi level compared to pure $LiFePO_4$. For transition metal ions doped at the Fe or Li sites, all of the PDOS show that the d orbitals of impurities are localized at the lower energy levels of the conduction band (CB). Additionally, it is ensured that the position of the valance band maximum (VBM) has not changed, although the VBM is a contribution of different atomic orbitals, thus the band gap of the doped compound does change

For Mn^{2+} doped at the Fe site, both the Mn 3d and Fe 3d orbitals are located at lower energy levels than the Fe 3d orbitals in pure $LiFePO_4$, resulting in a lower conduction band and decreased bandgap, as seen in Fig. 2(c). Interestingly, although the band gap value obtained by doping with Mn^{2+} (0.529 eV) is different from the reported value (0.39 eV [37]), the difference between the bandgap of pure $LiFePO_4$ (our calculated value is 0.74 eV and 0.61 eV [37]) and Mn^{2+}-doped $LiFePO_4$ is 0.211 and 0.22 eV, respectively. Because of the difference in calculation method and parameter setting, it is

reasonable that we only focus on their relative values. Specifically, from Fig. 3(a), it can be seen that the Al^{3+} doped at the Li site slightly increased the bandgap value (0.76 eV). Experimentally, Amin et al. [38, 39] reported that Al-doped $LiFePO_4$ has a higher ionic conductivity but slightly lower electronic conductivity compared to undoped $LiFePO_4$, which is consistent with our results. When Cr^{3+} is doped at the Li site, the Cr 3d orbital crosses the Fermi energy level, and the doped compounds show metallic characteristics, which is consistent with the results calculated by Shi S. [30]. Relevant experiments and calculations concerning Mo^{6+} dopants at the Fe site have also been performed. In this paper, the density of states of the Mo^{6+}-doped compounds indicates metallic characteristics, and related experiments also showed that the Mo^{6+}-doped compounds have stronger electronic conductivity. Although our calculated band gap values are somewhat different from those reported by Wang Yan [32], the calculated density of states all indicate that the Mo 4d electron states play an important role in the reduction in the band gap. To summarize, our calculated electronic structure and the current reported results are in basic agreement, further validating the reliability of the calculation model and the results.

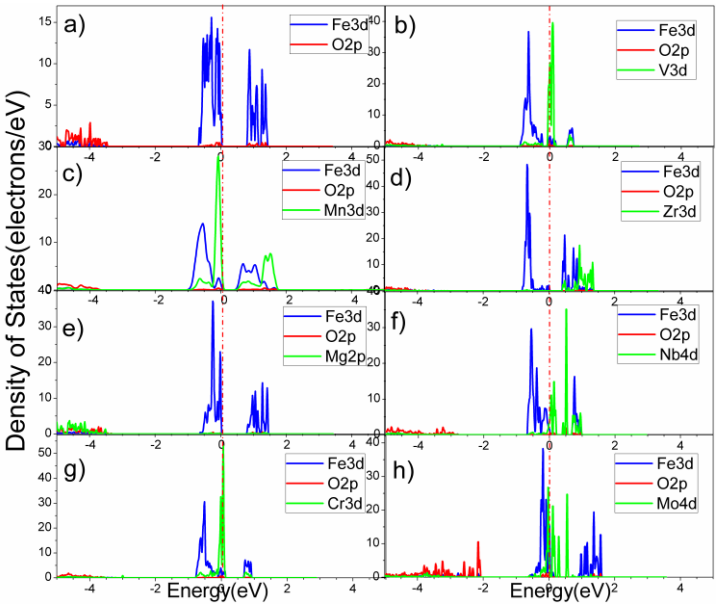

Figure 2. Partial density of states (PDOS) in a window of ±5 eV around the Fermi level where the Fe site was doped with (a) pure, (b) V^{3+}, (c) Mn^{2+}, (d) Zr^{4+}, (e) Mg^{2+}, (f) Nb^{5+}, (g) Cr^{3+}, or (h) Mo^{6+}. The Fermi energy level was set to zero (red dotted line).

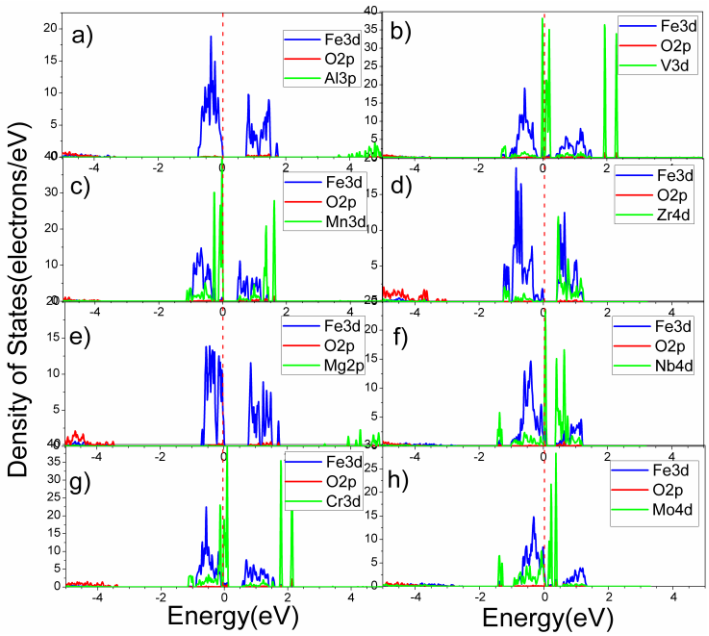

Figure 3. Partial density of states (PDOS) in a window of ±5 eV around the Fermi level where the Li site was doped with (a) Al^{3+}, (b) V^{3+}, (c) Mn^{2+}, (d) Zr^{4+}, (e) Mg^{2+}, (f) Nb^{5+}, (g) Cr^{3+}, or (h) Mo^{6+}. The Fermi energy level was set to zero (red dotted line).

3.3. Preferred dopant sites

To determine the most energetically preferable dopant lattice site of cation-doped $LiFePO_4$, models of different ions M^{n+} (n = 1~6) doped at the Li site and the Fe site were constructed. By comparing the calculated formation energy data, the preferential dopant sites were revealed, and the impact of ionic size and charge on its site occupation behavior was also analyzed. The formation energy (E_f) can be computed according to the following formula:

M^{n+} doped on Fe site:

$$E_f = E_{(LiFe_{1-n/16}M_{1/8}PO_4)} - E_{(LiFePO_4)} + \frac{n}{16}\mu_{Fe} - \frac{1}{8}\mu_M \qquad (1)$$

M^{n+} doped on Li site:

$$E_f = E_{(Li_{1-n/8}M_{1/8}FePO_4)} - E_{(LiFePO_4)} + \frac{n}{8}\mu_{Li} - \frac{1}{8}\mu_M \qquad (2)$$

where $E_{(LiFe1\text{-}n/16M1/8PO4)}$, $E_{(Li1\text{-}n/8FeM1/8PO4)}$, $E_{(LiFeMPO4)}$ represent the total energy of M^{n+} (n=1~6) doped at the Fe site and Li site and the total energy of pure $LiFePO_4$, respectively; μ_{Li} (μ_{Fe}, μ_{Fe}) is the chemical potential of a single Li (Fe, M) atom in the crystalline bulk; and n represents the charges of the doped M ions. The calculated formation energies of M^{n+} (n=1~6) doped on the Fe and Li sites are summarized in Table 2.

Table 2. The doped formation energy and bond population of M^{n+} (n=1~6) doped on the Fe site and Li site of $LiFePO_4$

Element	Charge	Ionic radius (pm)	Doped formation energy (eV)		Bond population	
			Fe site	Li site	Fe site(M-O)	Li site(M-O)

Na	1	102	/	0.1024		0.373
Co	2	65	0.0588	0.852	0.26	0.17
Mn		67	0.0558	0.841	0.258	0.177
Ni		69	0.021	0.854	0.22	0.152
Mg		72	-0.5756	0.227	1	1
Cu		73	-0.0077	0.7902	0.188	0.1
V		79	-0.1133	0.674	0.288	0.203
Al	3	53.5	-0.5865	0.5944	1	0.307
Co		54.5	-0.0018	1.066	0.25	0.193
Ni		56	0.0214	1.1286	0.227	0.17
Mn		58	-0.0063	1.069	0.268	0.2
Cr		61.5	-0.0545	1.0423	0.297	0.21
V		64	-0.268	0.828	0.303	0.23
V	4	58	-0.346	1.164	0.33	0.25
Zr		72	-0.722	0.897	0.362	0.257
V	5	54	-0.432	1.426	0.341	0.252
Nb		64	-0.433	1.4703	0.343	0.233
Mo	6	59	-0.129	2.0148	0.338	0.23

It can be seen from Table 2 that for all dopants, the formation energy of the doping on Fe sites is much lower than that of the Li sites, indicating that M^{n+} (n=2~6) preferentially incorporates into the Fe lattice of the $LiFePO_4$ structure. This is because M^{n+} doped at the Fe site forms a stronger covalent bond with surrounding oxygens than M^{n+} doped at the Li site. This can be further demonstrated by bond population analysis, as shown in Table 2. For any kind of ion doping on the Fe and Li sites, the bond population of M-O bonds formed on the Fe site is greater than Li site. The reason is that there are many more overlapped electrons between the M and O atoms, which indicates that a stronger interaction forms between dopants and adjacent O atoms. This can be directly visualized from the electron density distribution as shown in Fig. 7. In addition, for almost all ions, the formation energy of doping at Fe sites can be negative, which suggest that this process of doping is thermodynamically spontaneous. However, for all ions doped at Li sites, the doping process is thermodynamically nonspontaneous.

The calculated results are proved by relevant experimental results if available. For example, Roberts et al [40] reported that there was no evidence of magnesium doping at the Li site in samples prepared with the stoichiometry $Li_{1-x}Mg_xFePO_4$; however, samples prepared with the stoichiometry $LiFe_{1-y}Mg_yPO_4$ showed a linear decrease in cell volume with increased Mg dopants, indicating Mg is doping at the Fe site, which is consistent with Damian's results [41]. A series of experiments on vanadium doping have been carried out [42-47], and the results show that when vanadium is doped in different valence states, they were all preferentially occupied at the Fe site. These reports are consistent with our calculated results of V^{n+} incorporated into Fe lattices. Experimentally, Hong et al [30] reported that V doped at the P site instead; however, Omenya et al [46] later reported that the substitution at the P site could not be reproduced and that at least 10 mol% of the Fe sites were

occupied by V^{3+}. In addition, other cation dopants at the Fe site of $LiFePO_4$ have also been reported, such as Ni^{2+}, Co^{2+}, Mn^{2+}, Nb^{5+} [48,49], and Mo^{6+} [50-52]. In summary, whether doping with divalent or isovalent ions, the doping on the Fe site is more energetically favored and is thermodynamically spontaneous.

3.4. Correlations between dopant location and ionic radius or/and charge.

To reveal the factors influencing the diffusion and incorporation of dopant ions, the formation energy was compared in different aspects, and the relationship between the degree of ion doping and ionic radius or/and charges was studied.

Figure 4 suggests that for divalent ion doping, the doping formation energy decreases with increasing ionic radius at both the Fe and Li sites. Thus, ions are more easily incorporated into the lattice when their radius is closer to the host ionic radius (Fe^{2+}: 78 pm, Li^{+}: 76 pm). Similarly, trivalent ion (donor) doping is consistent with isovalent doping (except for Co^{3+} doped on the Fe or Li site), as shown in Fig. 5. It can be further confirmed that the above rule applies to cases of tetravalent (V^{4+}, Zr^{4+}) and pentavalent (V^{5+}, Nb^{5+}) ions doped at the Fe and Li sites, respectively. Non-transition metal ions such as Mg^{2+} and Al^{3+} will be discussed later.

As seen from Table 2, different valence ions with the same or similar ionic radius, such as V^{4+} (58 pm) and Mn^{3+} (58 pm); Zr^{4+} (72 pm) and Mg^{2+} (72 pm); V^{5+} (54.5 pm) and Co^{3+}(54 pm); Nb^{5+} (64 pm) and Co^{2+} (65 pm) lower the formation energy at Fe sites with increasing valency. Conversely, the formation energy increases with increasing valency if they are doped at the Li site. This indicates that the Fe site is more supportive of high-valent cation doping, while the Li site is more supportive of low-valent cation doping. This can be confirmed by related experiments and theory calculations; for example, Mo^{6+} preferentially dopes into the Fe site [31, 48], while Na^{+} tends to occupy Li sites [38, 53-54].

According to the above conclusion, when V^{n+} (n = 2, 3, 4, 5) with different charges are doped at the Fe and Li sites, the formation energy decreases with the increase of the ionic radius. However, for V^{n+} (n = 2, 3, 4, 5) doping at the Fe site, as shown in Fig. 6, the larger the radius is, the higher the formation energy because the charges on V^{n+} (n = 2, 3, 4, 5) are reduced. This finding suggests that ionic charge is the dominant factor in the attempted doping of Fe site of olivine phosphates and that the ionic size is secondary. For doping at the Li site, reducing the ionic charge and increasing the ionic radius work together to reduce the formation energy, which can be confirmed by the case of Na^{+} doped at the Li site. For all the ions doped at the Li site, Na^{+} has the lowest charge and the largest ion radius, and the formation energy is indeed the lowest of all the ions examined in this study.

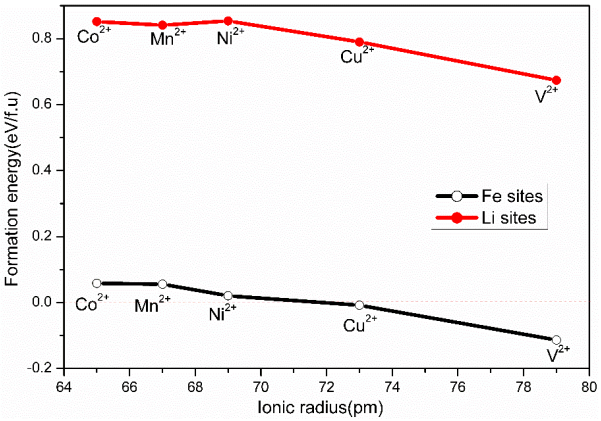

Figure 4. The formation energies of divalent dopants at Li and Fe sites as a function of ionic radius.

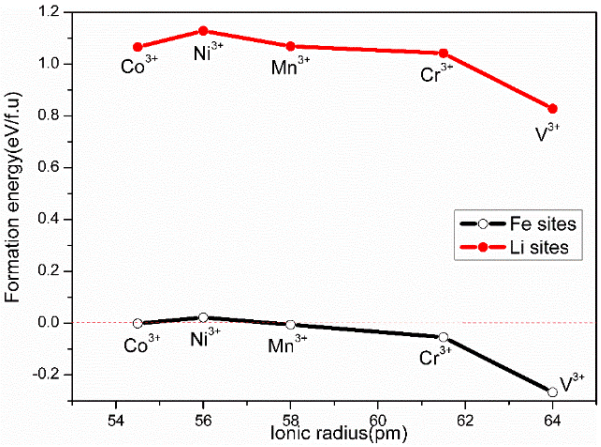

Figure 5. The formation energies of trivalent dopants on Li and Fe sites as a function of ionic radius.

It is worth pointing out that for the doping of transition metals and non-transition metal ions, the selected ions Mg^{2+}/Cu^{2+} and Al^{3+}/Co^{3+} with the same charge and similar radius are doped at the Fe and Li sites, respectively. As a result, the formation energy of non-transition metal ion doping is much lower than that of transition metals at both Fe and Li sites. This result indicates that the non-transition metal doping is more favorable from an energetic perspective. This is probably due to the presence of localized d electrons of the transition metal ions, which makes the Coulomb exclusion more significant when dopants incorporate into nearby sites. We can confirm the above speculation from the charge density distribution in Fig. 5. In Fig. 5 (b)~(d), Mg and Al have little electronic localization around them, while in Fig. 5(a), there is increased electron density on the Mg, even with lower valency than other ions.

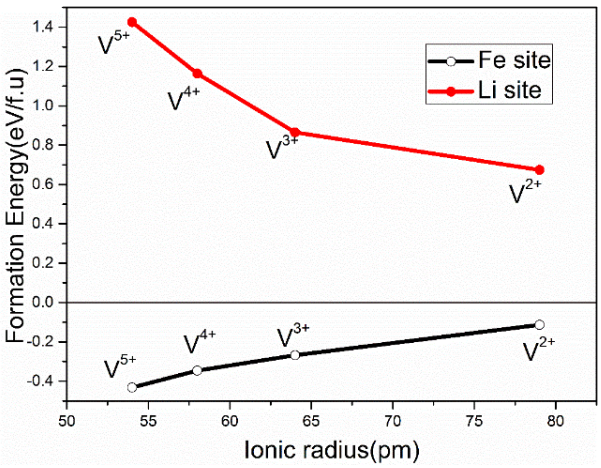

Figure 6. The formation energy of different valent V doped at Li and Fe sites as a function of ionic radius.

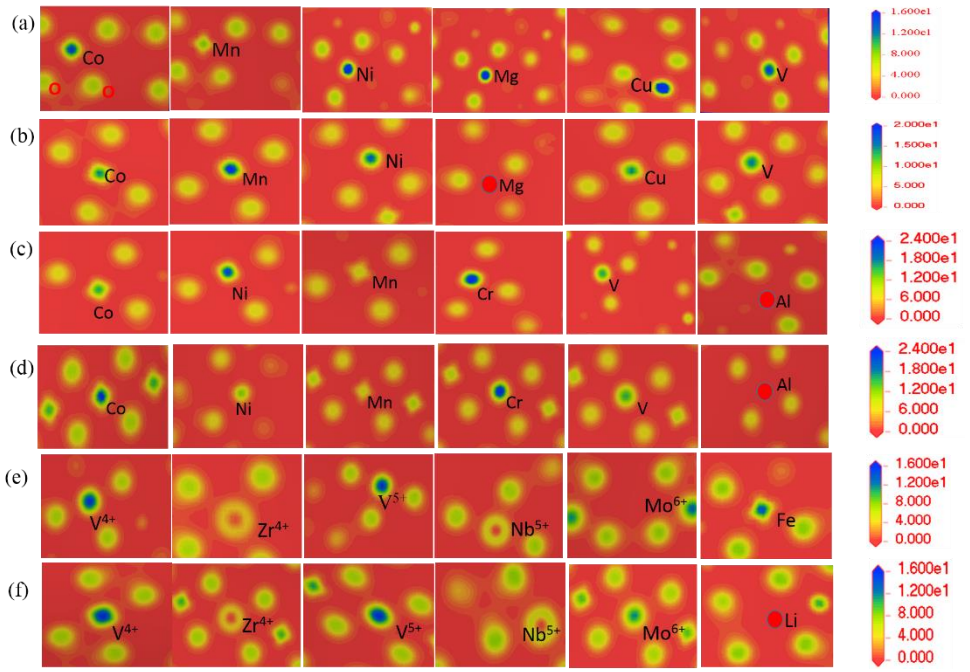

Figure 7. Charge density distribution of O-M-O (M=dopants) surfaces doped with different ions at the Fe and Li sites: (a) divalent ion doping at the Fe site, (b) divalent ion doping at the Li site, (c) trivalent ion doping at the Fe site, (d) trivalent ion doping at the Li site, (e) M^{n+} doping at the Fe site, and (f) M^{n+} doping at the Li site (n=4, 5, 6).

4. CONCLUSIONS

In this paper, a range of dopants with charges varying from +1 to +6 were studied by first-principles calculations, and the following main findings emerged from our investigation:

(1) For all ion doping, the formation energy of dopants at the Fe site can be much lower than dopants at the Li site due to the formation of a stronger covalent bond between the Fe site dopants and

adjacent oxygens. Moreover, almost all of the formation energies are negative when ions are doped at the Fe site and are positive when they are present at the Li site, indicating that the Fe site doping is thermodynamically spontaneous.

(2) With the increase of dopant ion radius, doping at the Fe site is easier, while Li site doping shows the opposite trend. In addition, the doping of Fe sites better favors high-valent ions, while the Li sites better support low-valent dopant ions.

(3) For different ion-doped $LiFePO_4$ materials, the charge of doped ions is the dominant factor that determines the formation energy of the doping process, and the ion size is secondary. Furthermore, from an energy perspective, non-transition metal ion doping is more prone to occur than transition metal doping.

ACKNOWLEDGEMENTS
This Study was supported by the National Key R&D Program of China (2017YFC0210406), the National Science Foundation of China (51772333, 51674300, 61533020), and the Fundamental Research Funds for the Central Universities of Central South University (2018zzts433). In addition, we also acknowledge the software support of the National Supercomputing Center in Shenzhen, China.

References

1. G. Ceder, Y.M. Chiang, D.R. Sadoway, M.K. Aydinol, Y.I. Jiang, B. Huang, *Nature*, 392 (2007) 694.
2. J. Kim, A. Manthiram, *Nature*, 390 (1997) 265.
3. J.M. Tarascon, M. Armand, *Nature*, 414 (2001) 359.
4. H. Shimoda, B. Gao, X.P. Tang, A. Kleinhammes, L. Fleming, Y. Wu, O. Zhou, *Phys. Rev. Lett.*, 88 (2002) 015502.
5. A.K. Padhi, K.S. Nanjundaswamy, J.B. Goodenough, *J. Electrochem. Soc*., 144 (1997) 1188.
6. K.F. Hsu, S.Y. Tsay, B.J. Hwang, *J. Mater. Chem*., 14 (2004) 2690.
7. M.M. Doeff, Y. Hu, F. Mclarnon, R. Kostecti, *Off. Sci. Res. Inf. Tech. Rep*., 3 (2003) 311.
8. H. Huang, S.C. Yin, L.F. Nazar, *Electrochem. Solid St*., 4 (2001) A170.
9. Y. Zhang, P. Xin, Q. Yao, *J. Alloy. Compd.,* 74 (2018) 404.
10. F. Croce, A.D. Epifanio, J. Hassoun, A. Deptula, T. Olczac, B. Scrosati, *Electrochem. Solid St*., 5 (2002) A47.
11. S.Y. Chung, J.T. Blocking, Y.M. Chiang. *Nat. Mater.,* 1 (2002) 123.
12. X. Ou, G. Liang, L. Wang, S. Xu and X. Zhao, *J. Power Sources*, 184 (2008) 543.
13. S. Yang, Y. Liu, Y. Yin, H. Wang and C. Cui, *J. Inorg. Mater.*, 22 (2007) 627.
14. D. Arumugam, G.P. Kalaignan and P. Manisankar, *J. Solid State Electrochem,* , 13 (2009) 301.
15. H. Liu, Q. Cao, L.J. Fu, C. Li, Y.P. Wu, H.Q. Wu, *Electrochem. Commun.,* 8 (2006) 1553.
16. H.C. Shin, S.B. Park, H. Jang, K.Y. Chung, W.I. Cho, C.S. Kim, B.W. Cho, *Electrochim. Acta,* 53 (2008) 7946.
17. R. Amin, C. Lin, J. Maier, *Phys. Chem. Chem. Phys*., 10 (2008) 3519.
18. G. Wang, Y. Cheng, M. Yan, Z. Jiang, *J. Solid State Electrochem.*, 11 (2007) 457.
19. S. Wu, M. Chen, C. Chien, Y. Fu, *J. Power Sources,* 189 (2009) 440.
20. L. Li, X. Li, Z. Wang, L. Wu, J. Zheng, H. Guo, *J. Phys. Chem.Solids*, 70 (2009) 238.
21. Y.M. Chiang, N. Meethong, Y.H. Kao, S.A. Speakman, *Adv. Funct. Mater*., 20 (2010) 186.
22. L. Hou, G. Tao. *Phys. Status Solid,* 254 (2017) 1700041.
23. C.S. Sun, Z. Zhou, Z.G. Xu, D.G. Wang, J.P. Wei, X.K. Bian, J. Yan, *J. Power Sources*, 193 (2009) 841.
24. J. Hong, C.S. Wang, X. Chen, S. Upreti, M.S. Whittingham, *Solid-State Lett*., 12 (2009) A33.

25. Z.D. Gao, Z.X. Bing, X. Jian, T. Jian, Z.T. Jun, C.G. Shao, *Acta Phys.-Chim. Sin*., 22 (2006) 840.
26. Z. Li, Z. M. Shou, W. D. Dan, S. Ou, D. Rui-Ping, M. Jian, *Chem.*, 25 (2009) 1724.
27. Y. Chen , Z.L. Wang, C.Y. Yu, D.G. Xia, Z.Y. Wu, *Acta Phys- Chim Sin*., 24 (2008) 1498.
28. M.S. Islam, D.J. Driscoll, C.A. J. Fisher, P.R. Slater, *Chem. Mater,* 17 (2005) 5085.
29. M.Wagemaker, B.L. Ellis, H.D. Luetzenkirchen, F.M. Mulder, L.F. Nazar, *Chem. Mater*., 20 (2008) 6313.
30. K. Hoang, M. D. Johannes, *J. Power Sources*, 206 (2012) 274.
31. S. Shi, L. Liu, C.Ouyang, D. Wang, Z. Wang, L. Chen, X. Huang, *Phys. Rev*. B., 68 (2003) 195108.
32. Y. Wang, Z.S. Feng, J.J. Chen, C. Zhang, X. Jin, J. Hu, *Solid State Commun*., 152 (2012) 1577.
33. G. Kresse, J. Furthmüller, J. Hafner, *Phys. Rev.* B., 5 (1996) 11169.
34. J.P. Perdew, K. Burke, M. Ernzerhof, *Phys. Rev. Lett*., 77 (1996) 3865.
35. K. Laasonen, R. Car, C. Lee, D. Vanderbilt, *Phys. Rev.* B., 43 (1991), 6796.
36. F. Zhou, M. Cococcioni, C.A. Marianetti, D. Morgan, G. Ceder, *Phys. Rev*. B., 70 (2004) 35.
37. J. Xu, G. Chen, *Physica* B., 405 (2010) 803.
38. R. Amin, C. Lin, J. Maier, *Phys. Chem. Chem. Phys*., 10 (2008) 3519.
39. R. Amin, C. Lin, J. Maier, *Phys. Chem. Chem. Phys*., 10 (2008) 3524.
40. M. R. Roberts, G. Vitins, J. R. Owen, *J. Power Sources*, 179 (2008) 754.
41. D. Goonetilleke, T. Faulkner, V.K. Peterson, N, Sharma, *J. Power Sources*, 394 (2018) 1.
42. J. Ma, B. Li, H. Du, C. Xu, F. Kang, *J. Electrochem. Soc*., 158 (2011) A26.
43. N. Gu, H. Wang, Y. Li, H. Ma, X. He, Z. Yang, *J. Solid State Electr*. 18 (2014) 771.
44. L.L. Zhang, G. Liang, A. Ignatov, M.C. Croft, X.Q. Xiong, I.M. Huang, Y.H. Huang, X.L.Hu, W.X. Zhang, Y.L. Peng, *J. Phys. Chem*. C., 115 (2011) 13520.
45. J. Hong, C. S. Wang, X. Chen, S. Upreti, M.S. Whittingham, *Solid-State Lett*. , 12 (2009) A33.
46. F. Omenya, N.A. Chernova, S. Upreti, P.Y. Zavalij, K.W.Nam, X.Q. Yang, M.S. Whittingham, *Chem. Mater.*, 23 (2011) 4733.
47. I.D. Johnson, M. Lubke, Y.O. Wu, N.M. Makwana, G.J. Smales, H.U. Islam, R.Y. Dedigama, *J. Power Sources*, 302 (2016) 410.
48. I.D. Johnson, M. Lubke, Y.O. Wu, N.M. Makwana, G.J. Smales, H.U. Islam, R.Y. Dedigama, *J. Power Sources,* 326 (2016) 476.
49. A. Zhang, A. Li, J. Xia, Z. Shao, *Int. J. Electrochem. Sci.,* 13 (2018) 5243.
50. D. Wang, H. Li, S. Shi, X. Huang, L. Chen. *Electrochimi. Acta*., 50 (2005) 2955.
51. D. Zhang, P. Zhang, J. Yi, Q. Yuan, J. Jiang, Q. Xu, Z. Luo, X. Ren, *J. Alloy. Compd*., 509 (2011) 1206.
52. H. Gao, L. Jiao, W. Peng, G. Liu, J. Yang, Q. Zhao, Z. Qi, Y. Si, Y. Wang, H.Yuan, *Electrochim. Acta.*, 56 (2011) 9961.
53. X. Yin, K. Huang, S. Liu, H. Wang, H. Wang, *J. Power Sources*,195 (2010) 4308.
54. Y. W. Chen, J. S. Chen. *Int. J. Electrochem. Sci*., 7 (2012) 8128.